Chapter 6

POD of 3D driven cavity

6.1 Introduction

In this chapter the POD eigenfunctions of the flow in a 3D driven cavity are presented. There are no homogeneous directions, so a full 3D POD has been computed. The snapshots used to compute the eigenfunctions are taken from the DNS of Chapter 3. The symmetry plane at z=0.5 is used to double the number of snapshots.

The Reynolds number for the DNS was Re=10,000. At this Reynolds number the flow is (weakly) turbulent, part of the power spectrum has a -5/3 slope. We have estimated the (correlation) dimension of the attractor using a time-series subtracted from the snapshots in the order of 10-20.

In Section 6.2 the symmetry of the 3D cavity is discussed. The POD eigenfunctions are discussed in Section 6.3. Finally some conclusions are presented in Section 6.4.

6.2 Symmetry considerations

Since the geometry and the boundary conditions are symmetric with respect to z=0.5, we have increased the number of snapshots by a factor of two by mirroring the snapshots. This is a cheap way to increase the number of snapshots. In addition, it enforces the POD eigenfunctions to be even or odd functions with respect to z=0.5, as they are analytically.

In general, we have to be careful with making use of symmetries in flow systems which have a preferred state. For some flow systems it is known that, depending of the initial position in state-space, the flow pattern can be different. The rotation direction of cells in the Rayleigh-Bérnard flow problem, for example, may never change in a simulation, whereas there are two different solutions known (see also [9] and references therein).

For the 3D driven cavity we found that the computed mean flow is not exactly symmetric, possibly due to the numerical method that was used. Despite the slight asymmetry we did make use of the symmetry plane because we expect no preferred state for the 3D driven cavity flow.

6.3 POD eigenfunctions

The POD eigenfunctions have been computed with the snapshot method of Sirovich (see Section 2.3). The snapshots are taken from the simulation described in Chapter 3. This simulation lasted 800 time units. The 320 snapshots which we have taken during this simulation constitute 8 Gigabytes of data. This large amount of data is difficult to handle, therefore it is cut into 80 pieces which are treated two by two to compute all innerproducts which form the matrix Q in equation (2.30).

For the snapshot method we would like to have uncorrelated snapshots. In Fig. 6.1 the autocorrelation of the snapshots is shown. The interval between two subsequent snapshots is 2.5 time units long. The autocorrelation at 2.5 time units is approximately 0.36, and after 5.0 time units the autocorrelation is approximately 0.12. Thus, the snapshots are slightly correlated. This is no serious problem, since the approximation of the space-correlation tensor does not get worse with extra snapshots.

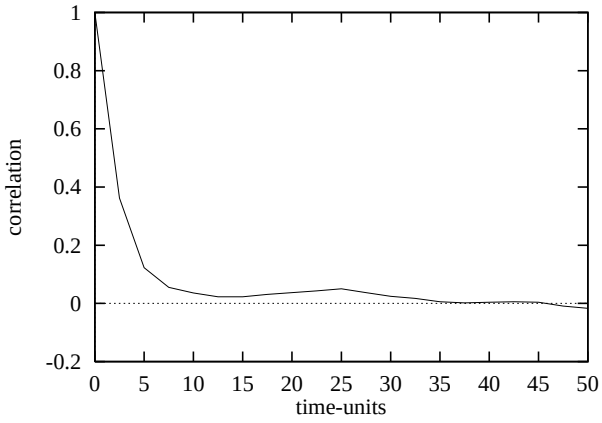

Figure 6.1: *Correlation of the snapshots in the database which is used to compute the POD eigenfunctions.*

The number of snapshots has been doubled to 640 as described in Section 6.2. The convergence of the eigenvalues as a function of the number of snapshots is shown in Fig. 6.2. The number of snapshots has been doubled for all number of snapshots. We can see that after some fluctuations at low number of snapshots the eigenvalues seem to converge. At 2x100 snapshots the second and third eigenvalue are very close to each other. We will see further on that they swap in the sense that the corresponding eigenfunctions swap. We will also see that the high energetic eigenfunctions do not change as much as their eigenvalues.

To further investigate the influence of the number of snapshots on the POD eigen-spectra we compared the spectra of 5 different sets of snapshots. We used 40, 160, and 320 snapshots, and also 2x160 and 2x320 snapshots by making use of the symmetry plane (the POD of the 2x160 set has been published in [11]). In Fig 6.3 the results for the first 80 eigenvalues are shown. The slopes of the spectra are approximately equal. In addition, it may be observed that the more snapshots are used the lower the eigenvalues become. This is due to the fact that the sum of the eigenvalues is equal to the average fluctuating energy which is approximately the same for all sets. This means that for an

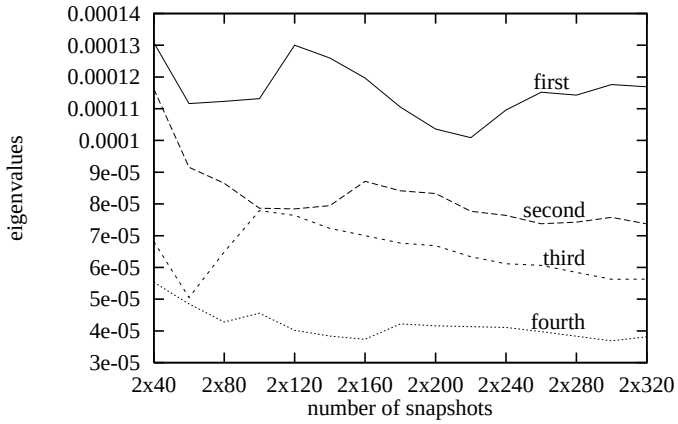

Figure 6.2: *Convergence of the POD eigenvalues as function of the number of snapshots.*

accurate approximation of the energy levels of the higher POD eigenfunctions we need more snapshots. This effect is not very strong in the first, say 10, POD eigenfunctions.

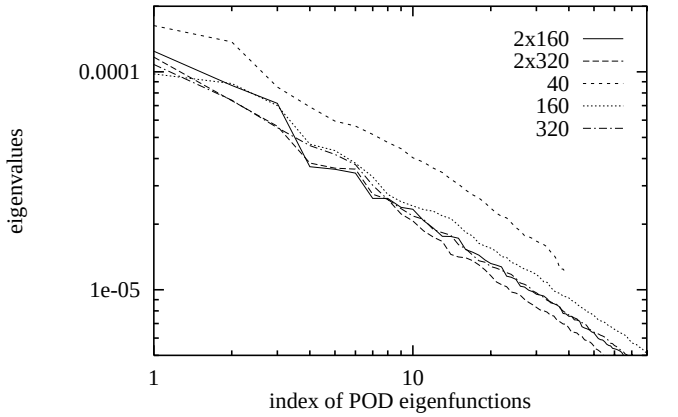

Figure 6.3: *POD eigenspectra of five different sets of snapshots.*

The POD eigenfunctions converge faster than their eigenvalues (in the sense that their high energy structures are formed) as shown in Fig. 6.4. For 2 sets of snapshots, namely 40 non-doubled and 160 doubled, the first two POD eigenfunctions have been plotted. Clearly the same structures are visible. Yet, their corresponding eigenvalues have changed in order of magnitude.

The difference between the first six POD eigenfunctions of the 2x160 set (see [11]) and the 2x320 set of snapshots is that the sixth one of the 2x160 set is the fourth one in the 2x320 set, and the fourth and fifth shift to fifth and sixth. The changing in order of magnitude of energy content of the fourth, fifth, and sixth eigenfunctions could be expected since for both sets of snapshots these eigenfunctions have almost the same energy content (see Table 6.1). We expect that the first POD eigenfunctions and eigenvalues do not change much if more snapshots are used, and that the other POD eigenfunctions with higher index remain eigenfunctions, but their index may change.

Some eigenvalues that have been computed using 2x320 snapshots are shown in Table 6.1. We can see that the first POD eigenfunction contains on average 7.5% of the energy.

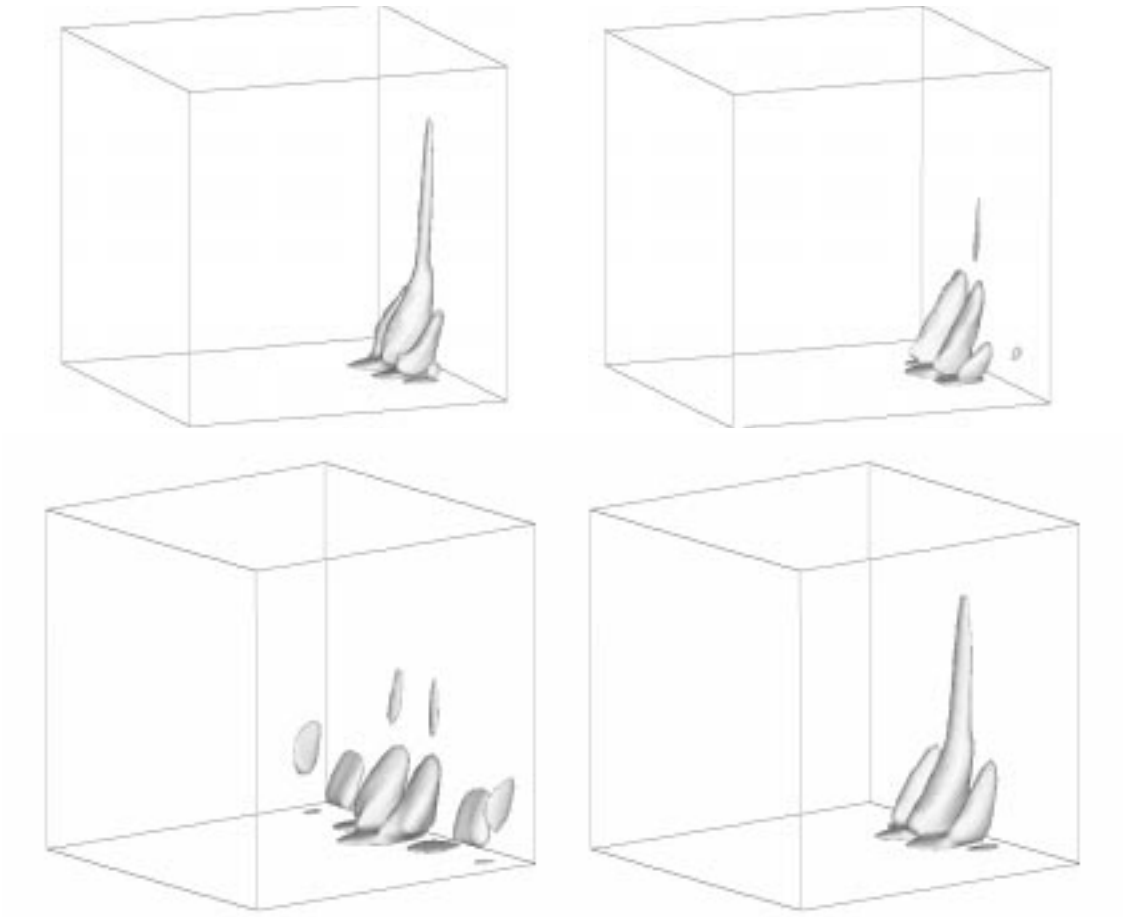

Figure 6.4: *High energy iso-surfaces of the first two POD eigenfunction for different sets of snapshots. The upper left- en right-hand plots are respectively the first and second POD eigenfunction with 40 non-doubled snapshots, and the lower left- and right-hand plots are respectively the first and second POD eigenfunction with 160 doubled snapshots. Notice that they have changed order.*

The first twenty-five eigenfunctions contain 42%, the first hundred contain 62.2%, and for 95% of the energy we need 454 POD eigenfunctions. This convergence in the 3D case is slower than in the 2D case, as shown in Fig. 6.5. For the first 10-20 POD eigenfunctions the decay rate is approximately the same, but for lower energy eigenfunctions the decay rate is much higher for the 2D case than for the 3D case. Therefore, it is likely that in 3D more POD eigenfunctions have to be retained in the dynamical system to mimic the DNS than in the 2D.

In Fig. 6.5 also a line with exponential decay proportional to $n^{-\frac{11}{9}}$ is shown. It was suggested by Knight *et al.* that the POD spectrum should exhibit such an exponential decay rate (see [28], and [37]). This suggestion can be viewed as a generalization of the Kolmogorov "-5/3" law (see Section 1.1). Fig. 6.5 shows that there indeed exists a small region where the exponential decay follows the "-11/9" slope.

In the figures 6.6 to 6.14 the first 20 POD eigenfunctions, and eigenfunctions with index 30, 40, 50, 60, 70, and 80 are shown. For each POD eigenfunction 4 plots are

index	λ_i	odd/even	% energy
1	$1.17 \cdot 10^{-4}$	odd	7.5%
2	$7.38 \cdot 10^{-5}$	even	12.2%
3	$5.63 \cdot 10^{-5}$	odd	15.9%
4	$3.82 \cdot 10^{-5}$	even	18.4%
5	$3.61 \cdot 10^{-5}$	even	20.7%
6	$3.58 \cdot 10^{-5}$	odd	23.0%
25	$9.64 \cdot 10^{-5}$	odd	42.0%
80	$3.65 \cdot 10^{-6}$	odd	62.0%
100	$2.96 \cdot 10^{-6}$	odd	66.2%
454	$5.70 \cdot 10^{-7}$	odd	95.0%

Table 6.1: *Some eigenvalues of 3D POD at Re=10,000. The right-hand column gives the cumulative percentage of the average energy.*

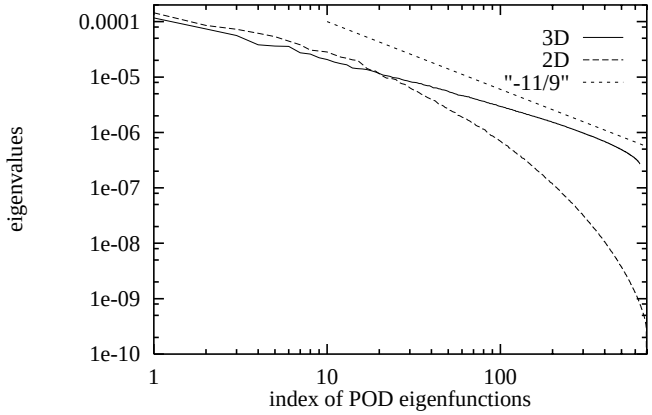

Figure 6.5: *The POD eigenvalues of the 2D and 3D POD, and the "-11/9" slope.*

shown, 2 iso-energy surfaces and 2 vector-plots in a y-z plane. All eigenfunctions $\boldsymbol{\sigma}^i$ have been normalized such that $(\boldsymbol{\sigma}^i, \boldsymbol{\sigma}^i)$=1.

All POD eigenfunctions possess a relatively high energy-level in the lower back-area at x=1. We will call this the downstream secondary eddy (DSE) location, as in the papers to which we will refer later on. Also in the middle of the downstream plane (DP) at x=1 we can observe high energies for most of the eigenfunctions.

The energy of the high energetic eigenfunction is concentrated in the DSE and DP location. The fourth eigenfunction (Fig. 6.7) is the first which has high energy-levels in the corners of the DSE and DP location at z=0 and z=1. This means that the largest fluctuations take place in the middle of the DSE and DP location.

The seventh and eighth eigenfunctions are the first which have areas with $|\boldsymbol{\sigma}^i(\boldsymbol{x})| \geq$ 3 close to the wall at x=0. All eigenfunctions with index larger than 10 (Fig. 6.8-6.14) have large areas with $|\boldsymbol{\sigma}^i(\boldsymbol{x})| \geq 1$. So, the fluctuations close to the wall at x=1 are smaller than the fluctuations in the corners DP at z=0 and z=1.

The first two POD eigenfunctions form, just like in 2D, a pair. In the third row of Fig. 6.6 vector-plots in the y-z plane at $x \approx 0.85$ are shown. The eddy structures in the middle

are obvious. They are a quarter out of phase. So, we can represent an eddy moving in the z-direction with the first two eigenfunctions.

The counter rotating eddy structures in the second eigenfunction are also visible in other eigenfunctions (Fig. 6.6-6.14). These counter rotating eddy structures look like Taylor-Görtler vortices. These Taylor-Görtler like (TGL) vortices have also been observed in experiments [1] [42] and in numerical simulations [19], at lower Reynolds numbers. At Re=10,000 Prasad and Koseff [42] could not discern TGL vortices, but they visualized single vortices. A single vortex is present in the first eigenfunction (Fig. 6.6). Moving TGL vortices in spanwise direction have also been observed in experiments and in numerical simulations at lower Reynolds numbers.

The size of the eddies is the largest for the first number of eigenfunctions. This means that the large eddies have the most energy, as expected. The eigenfunctions with somewhat higher indices have more counter-rotating eddies. For example the sixth one (Fig. 6.7) has 7 counter-rotating eddies. The eigenfunctions with higher indices show less vortex structures, but the size of the eddies is not significantly smaller. Only the eigenfunctions with index 70 and 80 (fig. 6.14) have smaller sizes, but these eddies are less pronounced.

In the DP the iso-energy surfaces form vertical tubes. These tubular structures appear in different sizes, as can be seen in the vector-plots shown in the fourth row of Fig. 6.6-6.14. These vector-plots show that the velocities at the tubes are large in vertical direction, and oscillate in the z-direction. The period of the oscillation changes with the eigenfunctions: high-energetic POD eigenfunctions have mostly long periods. It may be noted that the period of oscillation in the z-direction corresponds to the number of TGL vortices.

For homogeneous directions the POD reduces to a Fourier decomposition. So, the oscillating behavior in the z-direction of especially the v-velocity component and less pronounced of the w-velocity (because the velocity fluctuations are smaller) is an indication of the homogeneity of the v- and w-velocity component in the z-direction at the DP.

The eigenfunctions with index 9, 10, 13, and 17 have large velocities at the top of the y-z-plane at $x \approx 0.975$ (Fig. 6.8-6.11). When we look at the corresponding iso-energy surfaces $|\boldsymbol{\sigma}^i(\boldsymbol{x})|=1$ in these figures we can observe structures at the wall $y=1$ which look like the the iso-energy surfaces $|\boldsymbol{\sigma}^i(\boldsymbol{x})|=3$ of the first two eigenfunctions, only the scale is smaller. We have observed this phenomenon also in the 2D POD eigenfunctions, where the eigenfunctions with index 9 and 10 have the same vortex-structures in the upper-left corner as the first two eigenfunctions in the lower-right corner (see Fig. 4.4).

The 3D POD eigenfunctions with indices higher than 20 (Fig. 6.13-6.14) show a less organized structure than the eigenfunctions with index up to 20. It is clear that they possess more small-scale structures.

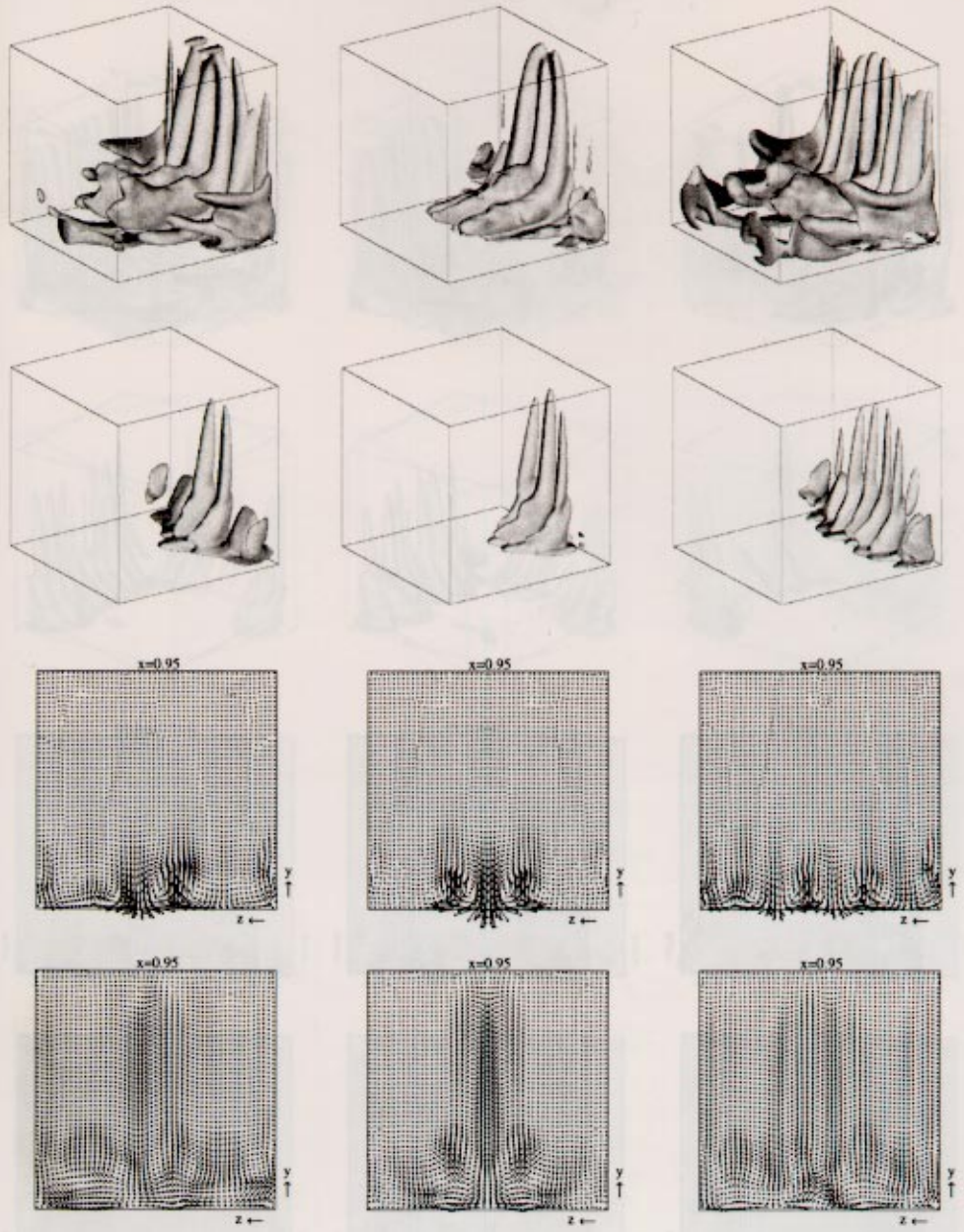

Figure 6.6: *The first three POD eigenfunctions. The first column of plots is the first, the second column of plots the second, and the last column of plots the third. All eigenfunctions are scaled to* $(\boldsymbol{\sigma}^i, \boldsymbol{\sigma}^i)=1$. *The two rows on top are plots of iso-energy surfaces. In the first row the iso-surfaces* $|\boldsymbol{\sigma}^i(\boldsymbol{x})|=1$ *and the second row* $|\boldsymbol{\sigma}^i(\boldsymbol{x})|=3$ *are shown. The plots in the bottom two rows are velocity vectors in a cross-section in the y-z plane: third row at* $x \approx 0.85$ *and last row at* $x \approx 0.975$.

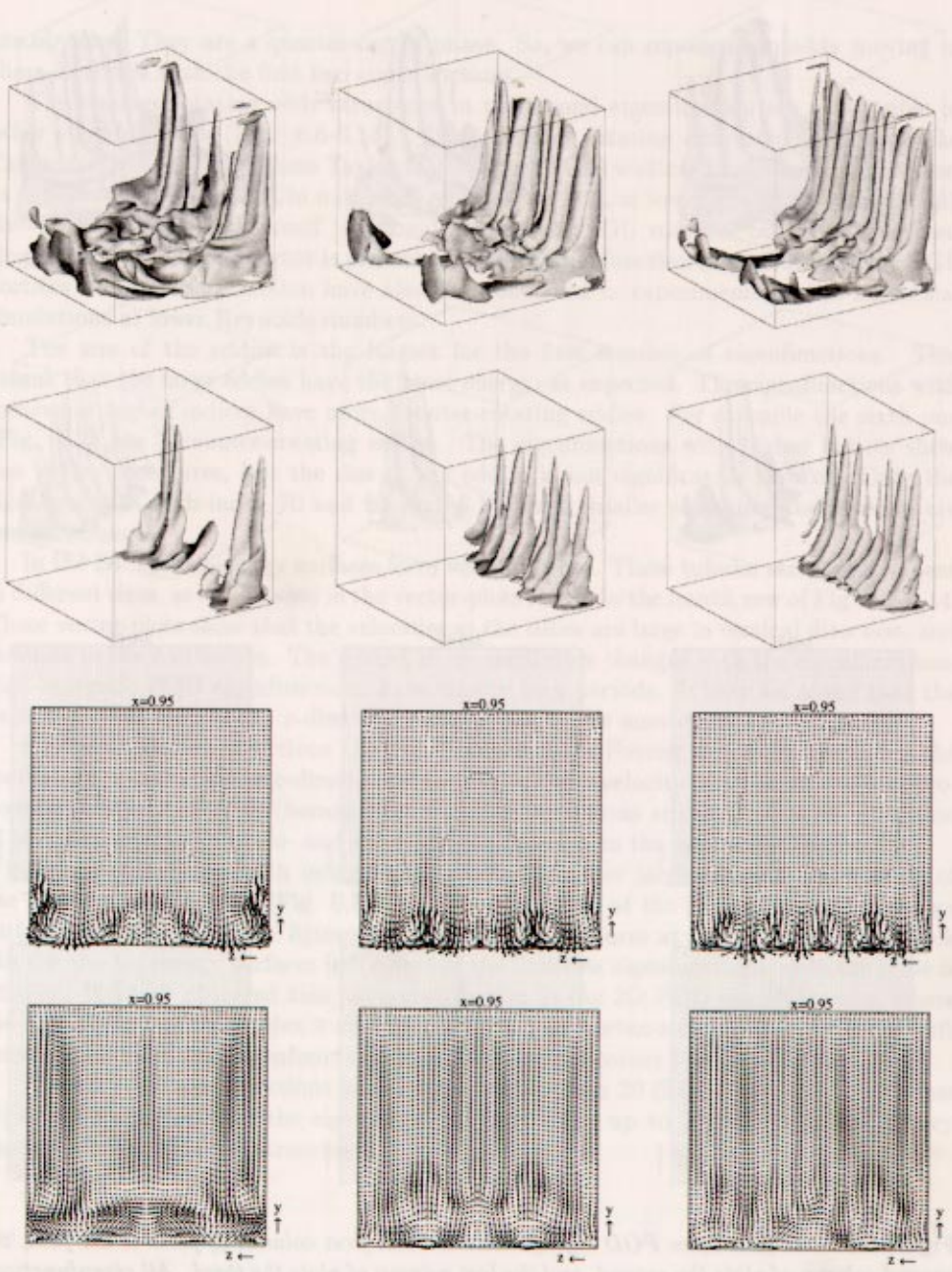

Figure 6.7: *As Fig. 6.6 but now POD eigenfunction with index 4, 5, and 6.*

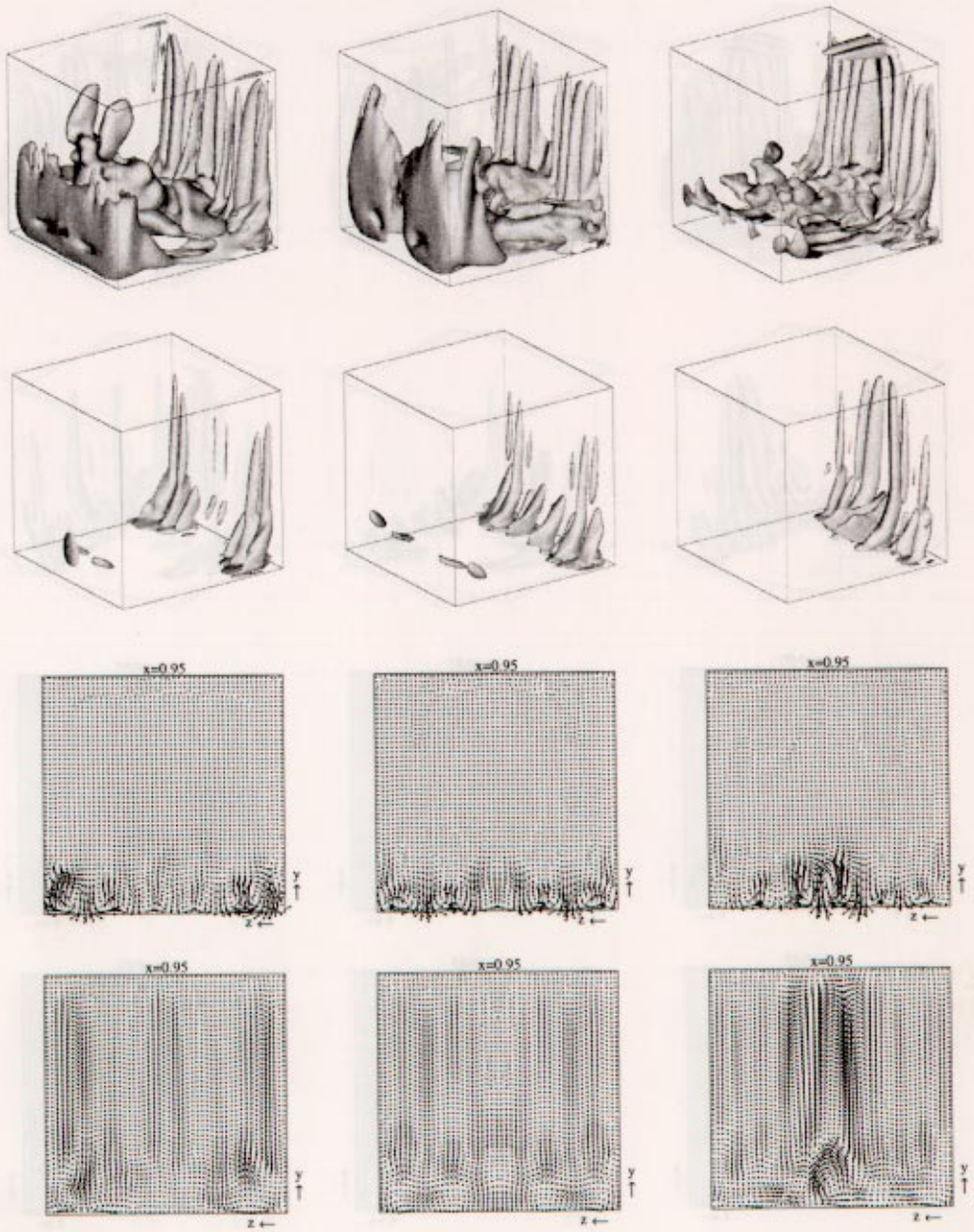

Figure 6.8: *As Fig. 6.6 but now POD eigenfunction with index 7, 8, and 9.*

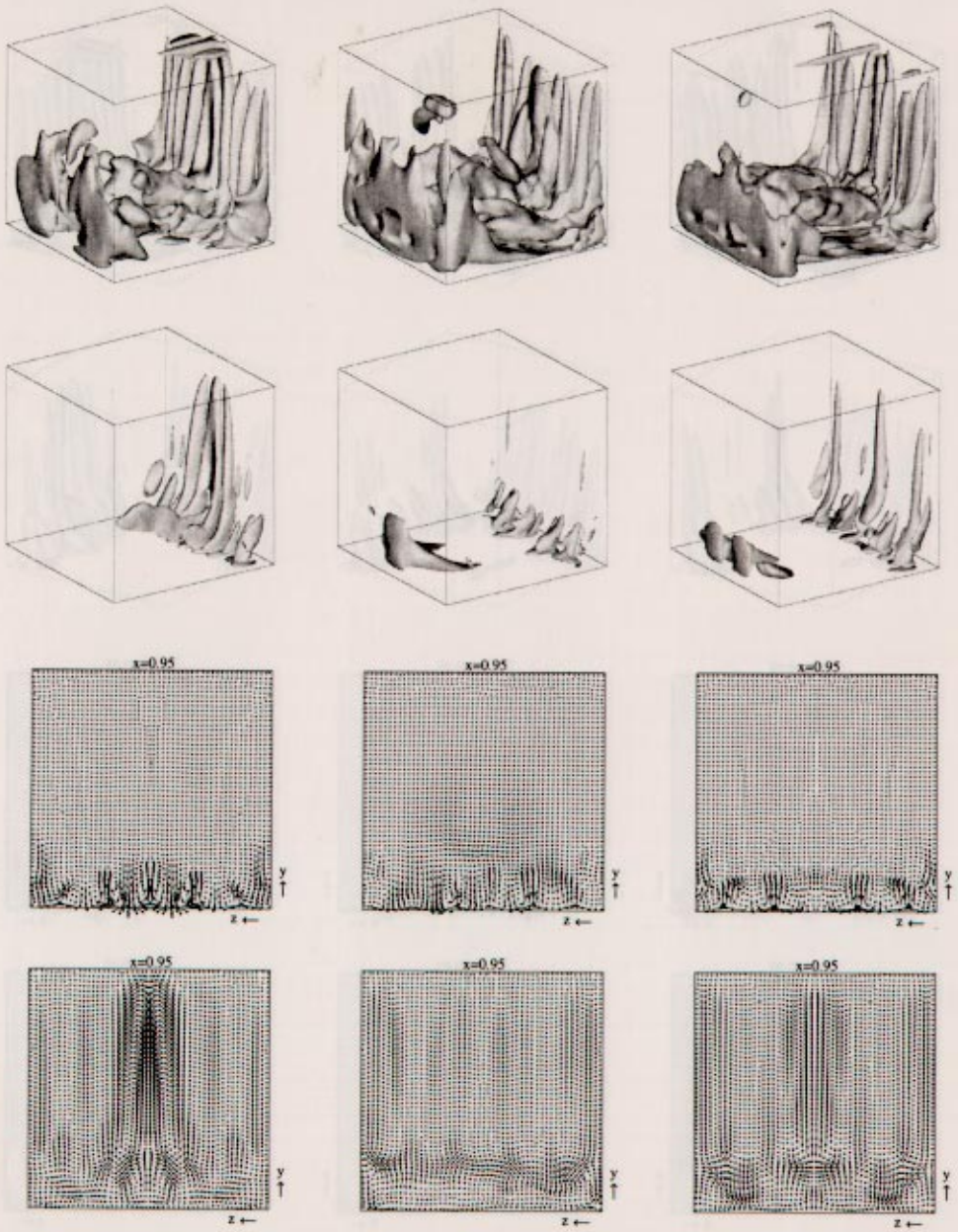

Figure 6.9: *As Fig. 6.6 but now POD eigenfunction with index 10, 11, and 12.*

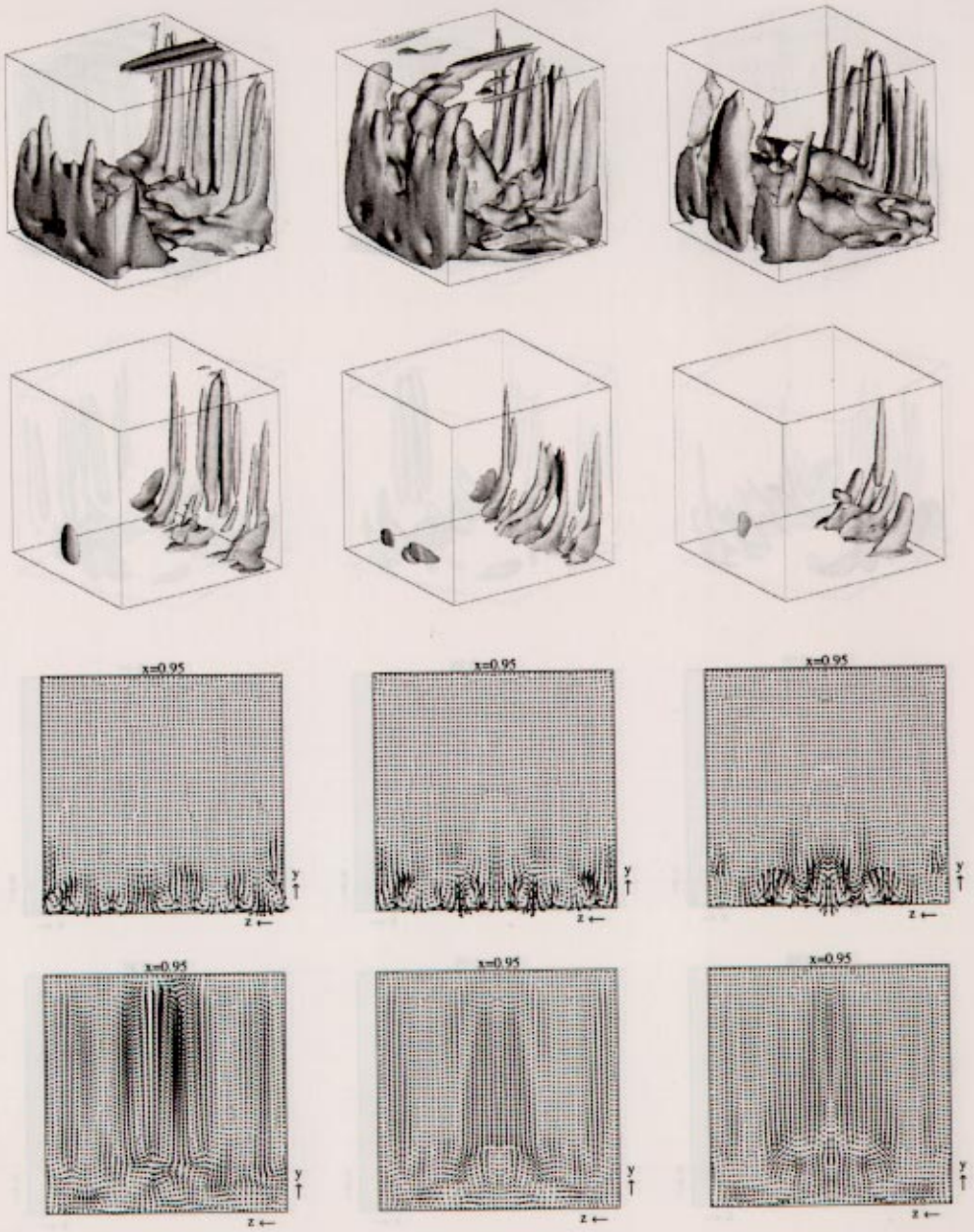

Figure 6.10: *As Fig. 6.6 but now POD eigenfunction with index 13, 14, and 15.*

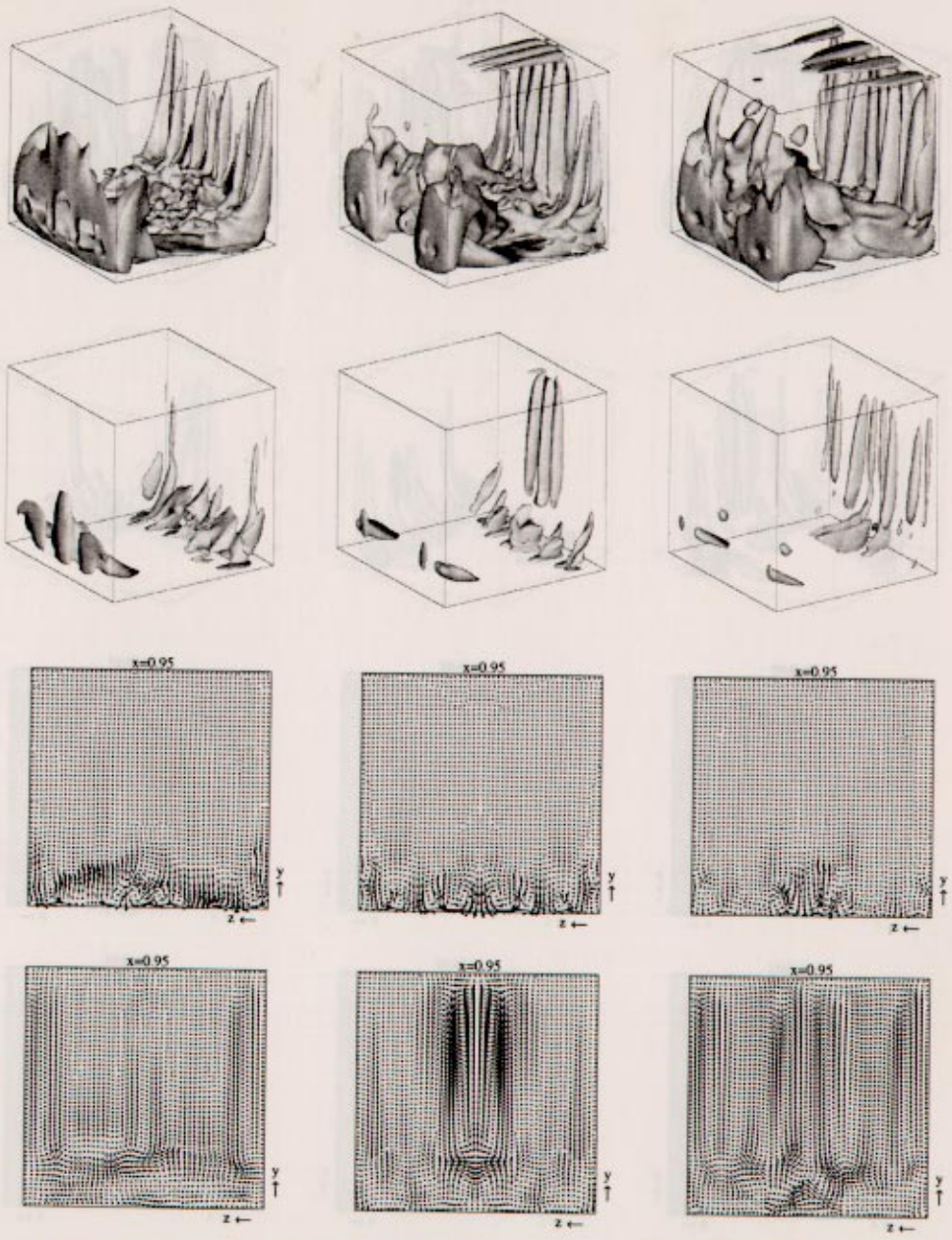

Figure 6.11: *As Fig. 6.6 but now POD eigenfunction with index 16, 17, and 18.*

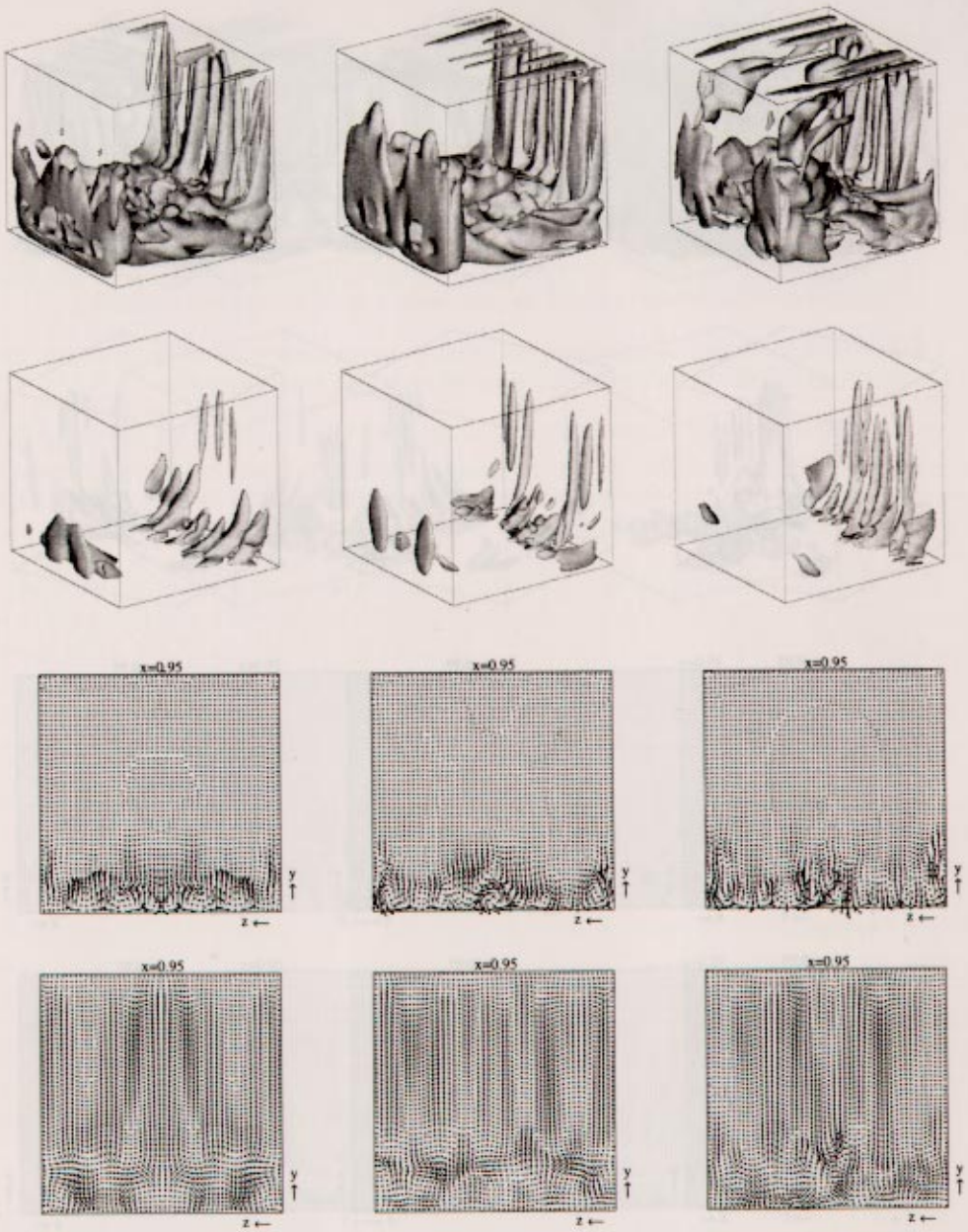

Figure 6.12: *As Fig. 6.6 but now POD eigenfunction with index 19,20, and 30.*

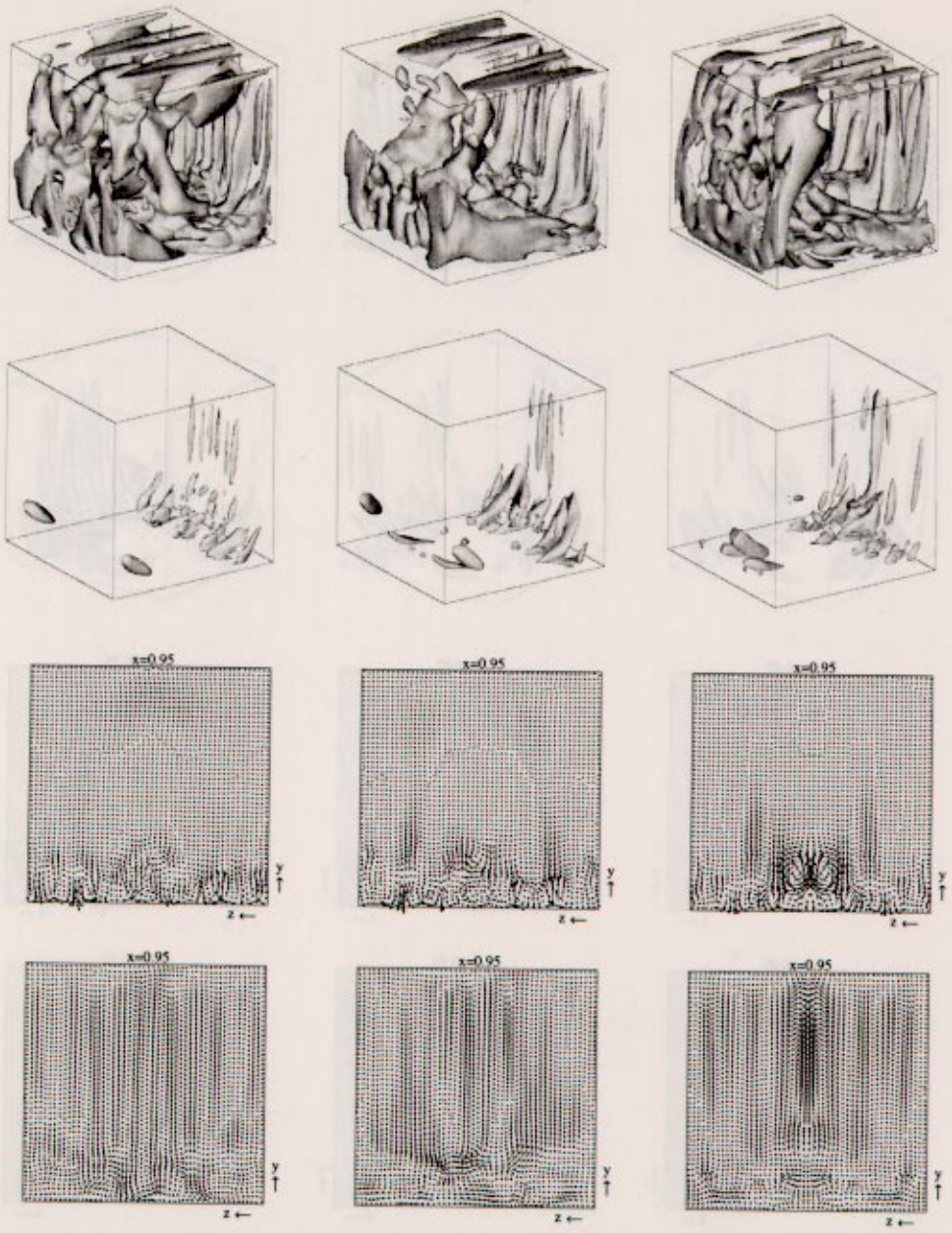

Figure 6.13: *As Fig. 6.6 but now POD eigenfunction with index 40, 50, and 60.*

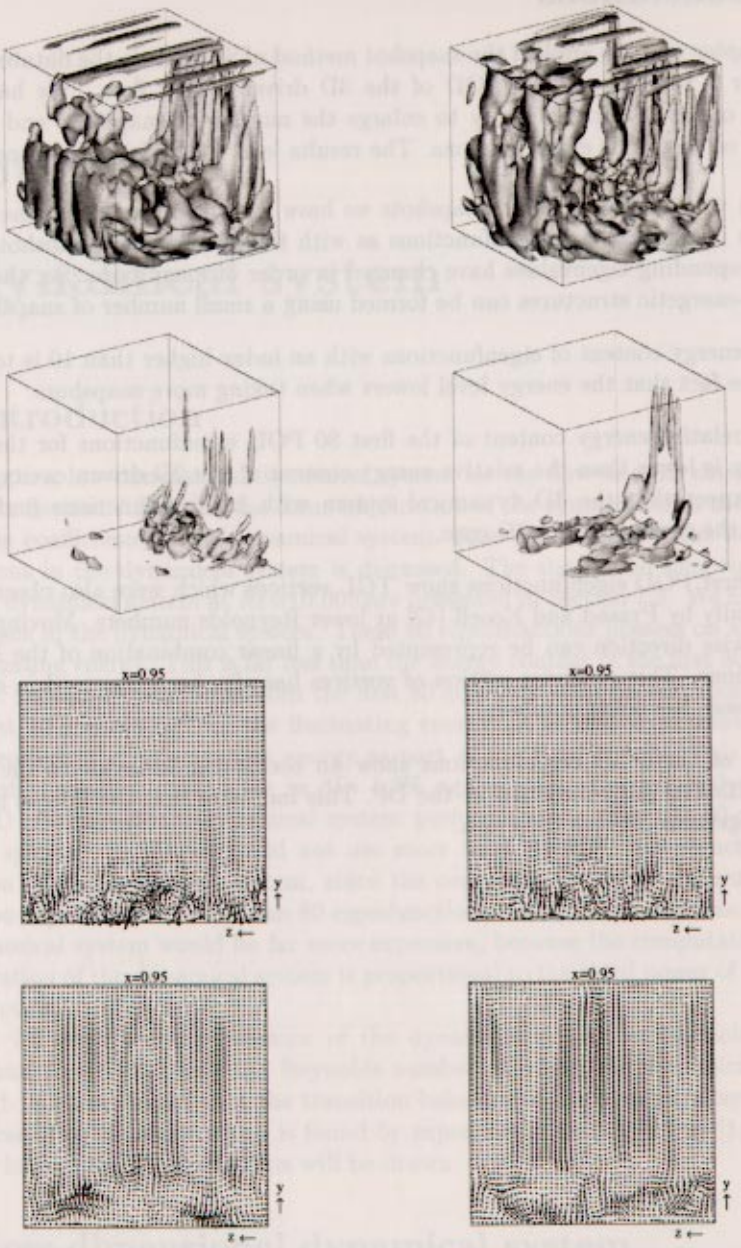

Figure 6.14: *As Fig. 6.6 but now POD eigenfunction with index 70 and 80.*

6.4 Conclusions

In this chapter we have applied the snapshot method of Sirovich to the database discussed in Chapter 3 to compute the POD of the 3D driven cavity flow. We have used the symmetry of the 3D driven cavity to enlarge the number of snapshots and to force the symmetry on the POD eigenfunctions. The results lead to the following conclusions.

- Even with 40 non-doubled snapshots we have found the same high-energetic structures in the first two eigenfunctions as with the 320 doubled snapshots. Only the corresponding eigenvalues have changed in order of magnitude. So, the large scale high-energetic structures can be formed using a small number of snapshots.
- The energy content of eigenfunctions with an index higher than 10 is too high, due to the fact that the energy level lowers when taking more snapshots.
- The relative energy content of the first 80 POD eigenfunctions for the 3D driven cavity is lower than the relative energy content of the 2D driven cavity. Therefore, we expect that the 3D dynamical system with 80 eigenfunctions performs worse than the corresponding 2D case.
- The first POD eigenfunctions show TGL vortices which were also observed experimentally by Prasad and Koseff [42] at lower Reynolds numbers. Moving vortices in spanwise direction can be represented by a linear combination of the POD eigenfunctions. This spanwise motion of vortices has also been observed in experiments (at lower Reynolds numbers).
- Most of the POD eigenfunctions show an oscillating behavior of the v- and w-velocities in the z-direction at the DP. This indicates that the flow is more or less homogeneous in that direction.